A Comparison of Optical Turbulence Models

Steve Doss-Hammel[a], Eun Oh[b], Jennifer Ricklin[c],
Frank Eaton[d], Charmaine Gilbreath[b], Dimitri Tsintikidis[a]

[a]SPAWAR Systems Center San Diego, code 2858, San Diego CA
[b]Naval Research Laboratory, Washington DC
[c]Army Research Laboratory, Adelphi MD
[d]Air Force Research Laboratory, Albuquerque NM

ABSTRACT

The U.S. Navy has an interest in the use of laser systems for surface ships. Such systems must operate within a thin near-surface environment called the marine atmospheric surface layer. There exist substantial gradients in temperature and momentum within this layer which make turbulence a strong function of height. We are interested in robust and simple optical turbulence models that can be used to predict turbulence along near-horizontal paths. We discuss several different models that are based upon similarity theory, and we compare the models with field transmission data taken from both over-water and over-land propagation paths.

1. INTRODUCTION

There are several envisioned uses of laser systems within the U.S. Navy. The high bandwidth capacity of point-to-point laser communications systems is an appealing concept. Similarly the use of a high energy laser for ship defense promises great versatility, since such a system permits speed-of-light delivery to a target. It also permits graduated engagements that could range from a simple disruption of activity to destruction.

In this paper we discuss the analysis of the performance of a laser system within the marine atmospheric surface layer. Determination of the refractive index structure parameter C_n^2 is the most important predictor of the effects of optical turbulence on beam quality, and we will focus on a comparison between models and measurements of C_n^2.

Almost all modern models for turbulence prediction are based upon the Monin-Obukhov similarity theory. We will examine and critique two similarity-based models for C_n^2. The primary method for examination and critique of the model attributes is a direct comparison of two different models against field data.

The first data set considered is taken from a propagation test in the desert. This data simplifies the examination of the behavior of the model since each diurnal period includes strong stable and strong unstable components, and a very characteristic transition through neutral stability. Furthermore, aerosol attenuation is not a factor in most of the high desert data.

The second data set considered is taken from propagation over the ocean surface. For this data no prominent diurnal period appears in the data set, and both heat capacity and mixing are dominant factors.

2. FIELD TEST EQUIPMENT AND TEST PROTOCOL

The field data examined in this test was generated by a transmissometer-scintillometer comprising a blackbody source, a transmitting telescope, a receiving telescope and both a mid-wave detector (3.5μm–4.1μm) and a long-wave (9.8μm–11.3μm) detector. The two telescopes are nearly identical with f/4 20 cm primary mirrors and hence 80 cm focal lengths. The blackbody is operated at 1200°K with a 1 KHz chopper and a radio frequency (162.1 MHz) reference signal. The blackbody aperture is 6.4 mm yielding a field beam divergence of ≈ 8 milliradians.

Further author information: (Send correspondence to S.D.-H.)
S.D.-H. E-mail: stephen.doss-hammel@navy.mil, Telephone: 619-553-4578

Report Documentation Page		Form Approved OMB No. 0704-0188

Public reporting burden for the collection of information is estimated to average 1 hour per response, including the time for reviewing instructions, searching existing data sources, gathering and maintaining the data needed, and completing and reviewing the collection of information. Send comments regarding this burden estimate or any other aspect of this collection of information, including suggestions for reducing this burden, to Washington Headquarters Services, Directorate for Information Operations and Reports, 1215 Jefferson Davis Highway, Suite 1204, Arlington VA 22202-4302. Respondents should be aware that notwithstanding any other provision of law, no person shall be subject to a penalty for failing to comply with a collection of information if it does not display a currently valid OMB control number.

1. REPORT DATE **2004**	2. REPORT TYPE	3. DATES COVERED **00-00-2004 to 00-00-2004**
4. TITLE AND SUBTITLE **A Comparison of Optical Turbulence Models**		5a. CONTRACT NUMBER
		5b. GRANT NUMBER
		5c. PROGRAM ELEMENT NUMBER
6. AUTHOR(S)		5d. PROJECT NUMBER
		5e. TASK NUMBER
		5f. WORK UNIT NUMBER
7. PERFORMING ORGANIZATION NAME(S) AND ADDRESS(ES) **Naval Research Laboratory,4555 Overlook Avenue, SW,Washington,DC,20375**		8. PERFORMING ORGANIZATION REPORT NUMBER
9. SPONSORING/MONITORING AGENCY NAME(S) AND ADDRESS(ES)		10. SPONSOR/MONITOR'S ACRONYM(S)
		11. SPONSOR/MONITOR'S REPORT NUMBER(S)

12. DISTRIBUTION/AVAILABILITY STATEMENT **Approved for public release; distribution unlimited**

13. SUPPLEMENTARY NOTES

14. ABSTRACT

15. SUBJECT TERMS

16. SECURITY CLASSIFICATION OF:			17. LIMITATION OF ABSTRACT	18. NUMBER OF PAGES **11**	19a. NAME OF RESPONSIBLE PERSON
a. REPORT **unclassified**	b. ABSTRACT **unclassified**	c. THIS PAGE **unclassified**			

Standard Form 298 (Rev. 8-98)
Prescribed by ANSI Std Z39-18

The receiver system consisted of the telescope and both a long-wave infrared detector and a mid-wave infrared detector. The signal from the detectors was separated from the chopped carrier waveform by means of a lock-in amplifier system. The scintillation measurement procedure sampled and recorded the signal at a 300 Hz rate for 109 seconds. This measurement was performed every 15 minutes, 24 hours a day.

3. THE CHINA LAKE FIELD TEST: A TEST OVER LAND

A first set of turbulence data to be examined here is from a 9 day test period from 12 July 2001 through 20 July 2001 at the Naval Air Warfare Center at China Lake, CA. In spite of the name of the test location, the test range consists of a relatively homogeneous flat and dry lake-bed. These dates correspond to our time scale using day-of-year 193 through 201. The transmission path was a near-horizontal slant-path, with the receiver at a height of 22 m, and the transmitter height was 2 m. The path length for the data used in this paper was 3850 meters in range.

There were four distinct sites that served as sources for meteorological data for the test period. Two of the sources provided data over the full period of the test, and we have compared the two data sets. One source ('Tower 8') is approximately 10 km from the propagation path, and the second ('Air Field') is approximately 3 km distant. This is not an ideal configuration since one would hope for co-location of the meteorological and propagation measurements, but the homogeneity of the area (a large dry lake bed) and an inter-comparison of the data indicates that the larger scale events recorded in both meteorological data records is close to the actual propagation conditions. The ground surface temperature was recorded by an infrared radiometer located with 100 m of the receiver site.

The meteorological data is recorded at 5 minute intervals. We use either 3 point or 5 point averages for the meteorological data since the scintillation data is recorded at 15 minute intervals, and the synchronization between the meteorological clock and the scintillation clock is expected to have possible errors of several minutes.

4. COMPARISON

We chose data from the China Lake site because of the prominent meteorological features that appear: large daily solar insolation, and a large diurnal change in wind speed. This creates a pattern in the most important model input data and thus helps to isolate and partially de-couple some of the complex features in the model equations. The over-land data shows the diurnal solar insolation effects prominently, and in addition includes strong diurnal wind speed variations. The effects of the wind and the solar insolation can be distinguished, and both are apparent in the C_n^2 calculation.

Scintillation data was collected by our scintillometer along a shorter (1280 m) path, and by a saturation-resistant commercial scintillometer (made by Scintec), which provided unsaturated values of C_n^2 such that $\max\{C_n^2\} > 10^{-13} \mathrm{m}^{-2/3}$. The extent of the longer (3850 m) propagation path that is the source of the data investigated here, caused the C_n^2 data (plotted with squares in fig. 1) to show the effects of saturation; the mid-day values of $C_n^2 < 10^{-13} \mathrm{m}^{-2/3}$. In the comparison of model data with experimental data the first point to emphasize is the much larger variance of the model C_n^2 (shown as '+' signs) than of the field C_n^2 data. Note that the large excursions of the C_n^2 prediction can exceed $10^{-12} \mathrm{m}^{-2/3}$, and these values are well in excess of any of the measured maxima of C_n^2.

We will use the data for the 48-hour period of days 195-196 to examine the elements of the model. There is a fairly clear pattern to be seen in the divergence of the model and field data. The first feature to notice is the occurrence of minima in C_n^2 occurring ≈ 30 minutes after sunrise, and ≈ 30 minutes before sunset. The noteworthy features in fig. 1 are: 1) the field data (black squares) show the minima with the morning minima less strong than the evening, and the PAMELA model produces a stronger minimum at both points; 2) the large fluctuations in the modelled C_n^2 for the first half of the day (from 195.0 to 195.5, and from 196.0 to 196.5) that generate unrealistically large C_n^2 values; 3) a sustained and smooth, steady signal for the second half of each day that is slightly under-predicting the field C_n^2 values.
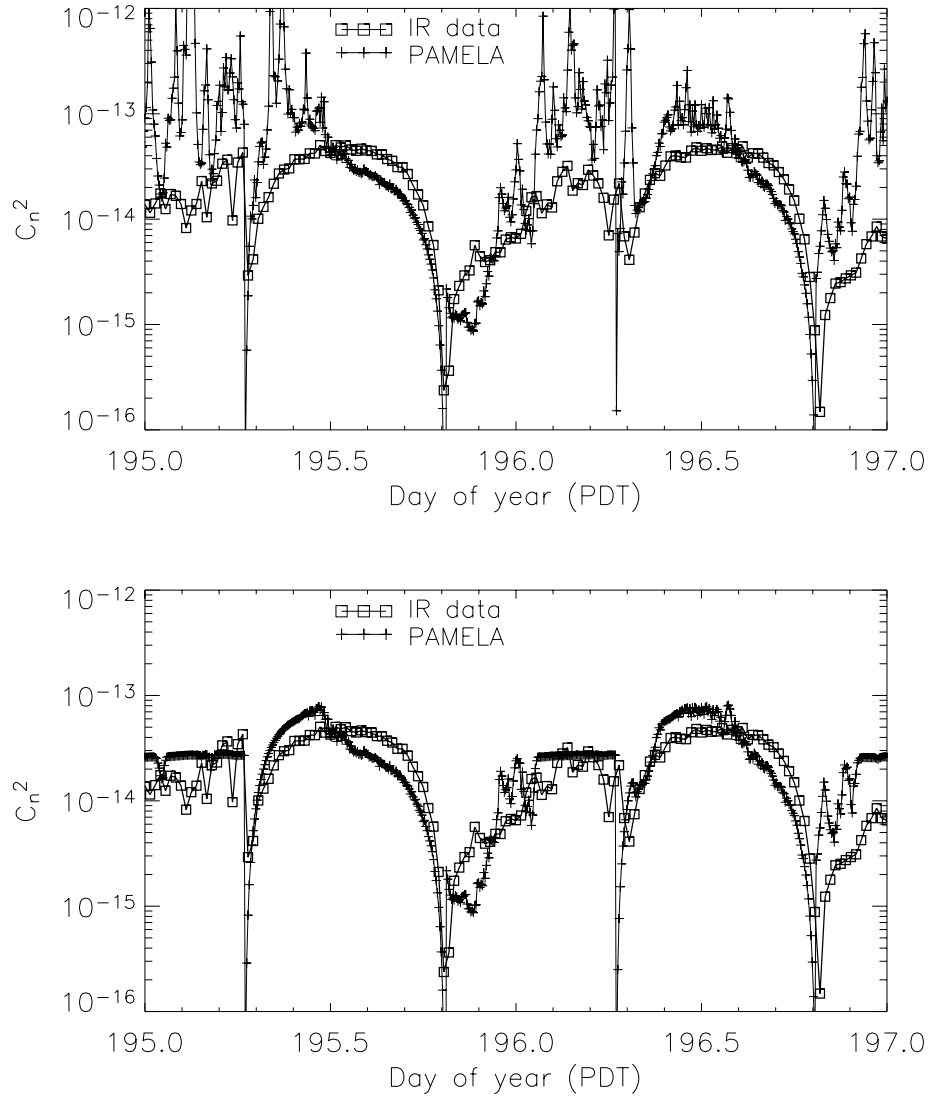
Figure 1. A 48-hour time series from transmission across the 3850 m path. C_n^2 determined by direct transmission measurements at $3.85\mu m$ is shown with the boxes, and PAMELA model data is shown with plus-signs. Note the prominent minima in C_n^2 occurring ≈ 30 minutes after sunrise, and ≈ 30 minutes before sunset. The upper panel shows C_n^2 for wind-speed threshold 0.1 m/s, while the lower panel shows C_n^2 calculated for wind-speed $= \max\{v_0, 2.5\}$.

5. PAMELA MODEL DETAILS

Solar irradiance R is calculated using the geographical and temporal inputs, via spherical astronomy calculations. The estimated solar irradiance R is used to determine the radiation class $c_r = R/300$. For a wind-speed v_0 define the wind-speed class $c_w = \min\{v_0/2, 4\}$ and then the Pasquill stability category P can be determined:

$$P = \frac{-(4 - c_w + c_r)}{2} \qquad (1)$$

The roughness length for the shrub-covered dry lakebed can be estimated from tables such as that found in Arya[1]: $z_r = 0.16$m, and from this it is possible to calculate the Obukhov buoyancy length scale L:

$$L = \left[(a_1 P + a_2 P^3) z_r^{-(a_3 - a_4 |P| + a_5 P^2)}\right]^{-1} \tag{2}$$

where

$$\begin{aligned} a_1 &= 0.004349, & a_2 &= 0.003724, \\ a_3 &= 0.5034, & a_4 &= 0.231, \\ a_5 &= 0.0325. \end{aligned}$$

The eddy viscosity (diffusivity) relations are defined next. For mean vertical velocity W and fluctuating part w, mean horizontal velocity U and fluctuating part u, define vertical momentum flux in terms of the eddy viscosity K_m:

$$\overline{uw} = -K_m \left(\frac{\partial U}{\partial z}\right) \tag{3}$$

For the mean potential temperature Θ and fluctuating part θ, define vertical heat flux in terms of the eddy diffusivity of heat K_h:

$$\overline{\theta w} = -K_h \left(\frac{\partial \Theta}{\partial z}\right) \tag{4}$$

For the mean specific humidity Q and fluctuating part q define the vertical water vapor flux using the eddy diffusivity of water vapor K_w:

$$\overline{qw} = -K_w \left(\frac{\partial Q}{\partial z}\right) \tag{5}$$

The dimensionless wind shear $\phi_m(\zeta)$ and the dimensionless potential temperature gradient $\phi_h(\zeta)$ are expressed as functions of the scaled buoyancy parameter $\zeta = z/L$. The turbulent exchange coefficients for heat K_h and momentum K_m are:

$$K_h = \frac{\kappa u_* z}{\phi_h(\zeta)} \quad \text{and} \quad K_m = \frac{\kappa u_* z}{\phi_m(\zeta)} \tag{6}$$

where $\kappa \simeq 0.4$ is the von Kármán constant. Note that in^2 $K_h = K_m$. From the wind speed v_0 and the roughness length z_r the friction velocity u_* is given by:

$$u_* = \frac{\kappa v_0}{\ln(z/z_r)} \tag{7}$$

and the characteristic temperature T_*

$$T_* = \frac{-H}{c_p \rho u_*} \tag{8}$$

is defined using the heat flux H, specific heat c_p, and mass density ρ. With pressure P_a measured in millibars, the atmospheric refractive index n:

$$n - 1 = \frac{77.6 \times 10^{-6} P_a}{T} \left(1 + \frac{7.52 \times 10^{-3}}{\lambda^2}\right) \tag{9}$$

The field data uses $\lambda = 3.85 \mu$m, and

$$\frac{dn}{dz} = -\frac{77.6 \times 10^{-6} P_a T_* \phi_h}{0.4 z T^2}$$

The eddy dissipation rate ϵ is:

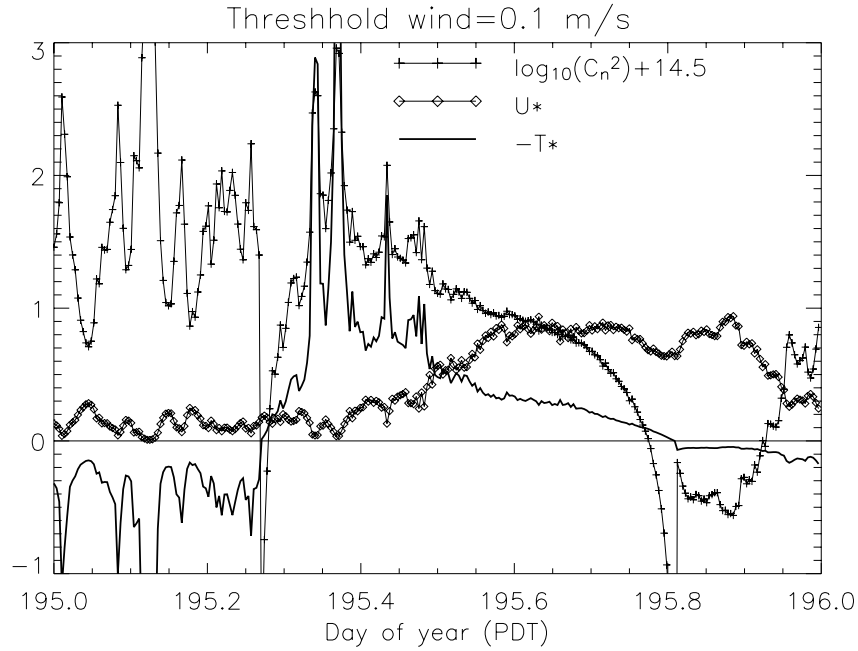$$\epsilon = \frac{u_*^3 (\phi_m - \zeta)}{0.4 z} \tag{10}$$

Figure 2. A comparison of T_*, u_*, and C_n^2 for a 24-hour period. For this data, the minimum wind speed threshold is set to 0.1 m/s.

and with the constant $b \approx 2.8$ we can evaluate C_n^2:

$$C_n^2 = \frac{bK_h}{\epsilon^{1/3}} \left(\frac{dn}{dz}\right)^2 \tag{11}$$

To elucidate these features, in fig. 2 the important elements T_*, u_*, and C_n^2 are compared. To facilitate the display of the graphs of the three quantities, the time domain for the comparison has been restricted to a 24-hour period: 195.0–196.0.

As noted in the figure legend, the C_n^2 curve is shown as $\log(C_n^2)$, and it has been shifted to overlay the graphs of T_* and u_*. As can be seen from eqns. (7) and (13), $C_n^2 \to \infty$ as wind-speed $v_0 \to 0$, so the minimum wind speed must be bounded away from zero. In fig. 2 the wind-speed threshold is 0.1 m/s. In this plot, we averaged the C_n^2 calculation over a 25-minute span to damp some of the more extreme spikes. This averaging was done simply to reduce the sharp fluctuations in the T_* and C_n^2 graphs. It is still the case that the C_n^2 calculation is highly fluctuating.

The other two curves are included to elucidate the factors in the behavior of the C_n^2 calculation. First, note that eqn. (7) implies that the fluctuations in the graph of u_* are essentially showing the variations of wind speed v_0. As the wind speed oscillates around a small value (the time from 195.0 to 195.3), there are large fluctuations induced in both T_* and in C_n^2. The direct relationship can be seen by expanding eqn. (11) as:

$$C_n^2 = 1.84b\phi_h \left(\frac{1}{\phi_m - \zeta}\right)^{1/3} \left(\frac{77.6 \times 10^{-6} P_a}{T}\right)^2 z^{-2/3} \underbrace{T_*^2} \tag{12}$$

$$= 1.84b\phi_h \left(\frac{1}{\phi_m - \zeta}\right)^{1/3} \left(\frac{77.6 \times 10^{-6} P_a}{T^2}\right)^2 z^{-2/3} \underbrace{\left(\frac{-H}{c_p \rho u_*}\right)^2} \tag{13}$$

For this model experiment, we hold the height $z = 10$m. The important variations in the signals C_n^2 and T_* are thus entirely produced by the fluctuations of the values of heat flux H and u_* which (see eqn. (7)) is just a

linearly scaled wind speed v_0. In the examination of the model behavior in the following sections, we will follow the values of the variables u_*, T_*, and H which are indicated by the under-braces in eqns. (12) and (13).

The point at which heat flux H changes sign is evident in fig. 2, since T_* changes sign at the same point. The effect of small values of u_* is also apparent for $195 \leq \text{time} \leq 195.5$: as u_* becomes small, both T_* and C_n^2 experience large spikes in value. Around noon, (195.5) the mean wind speed starts to increase. The effect on both C_n^2 and T_* is apparent in fig. 3 as the large fluctuations in the graphs of both are greatly reduced for time > 195.5.

6. DISCUSSION OF THE PAMELA MODEL

The difficulty with the PAMELA model is that removal of the sensitivity to wind speed, when the wind speed is low, is not a simple modification. If we insert a higher threshold for wind speed, as is done in fig. 3 the large scale fluctuations are still unrealistically strong. In the upper panel of fig. 3 the same data is shown for a wind speed threshold of 1.0 m/s, thus wind speed $v_0 = \min\{v_0, 1.0\}$ m/s. In this figure, the signal was also averaged to smooth out the data.

The effects of low wind-speed on C_n^2 become even more apparent when the wind speed threshold is increased to 2.5 m/s in the lower panel of fig. 3. Although this threshold ensures that the extreme values of the model C_n^2 are suppressed, many of the other legitimate dynamic elements of the signal are also removed by this process.

We recognize that there are other dependencies that affect the amplitude and shape of the C_n^2 prediction. We have not considered for example the contributions from dimensionless wind shear ϕ_m and the potential temperature gradient ϕ_h. But these are functions of the Monin-Obukhov length, and should not show the instantaneous effects of wind speed.

7. BEHAVIOR OF PAMELA FOR PROPAGATION OVER WATER

In this section we examine the application of the PAMELA model to the prediction of optical turbulence over the ocean. A data set generated from measurements on a 7 km path across Zuniga Shoals outside of San Diego Bay was used as the data for this test. A record of scintillation data over a two-day period is shown in fig. 4. The field test equipment for the scintillation measurements was quite similar to the system described in section 2 above. A scintillation measurement was made every 20 minutes, 24 hours per day throughout the test. Simultaneous meteorological measurements were made from a flux buoy anchored near the mid-point of the propagation path, including in particular air temperature, sea surface temperature, humidity and wind-speed measurements.

Note that the field data shows no evidence of the diurnal change in sign of the surface heat flux. The ocean has a very large heat capacity, and effective mixing processes. Thus solar insolation is only one of several important factors in the determination of sea surface temperature and subsequently $T_{\text{air}} - T_{\text{surface}}$. In fact $T_{\text{air}} - T_{\text{surface}} < 0$ can persist for days or weeks in an open ocean environment. For the comparison shown in fig. 4 we set the PAMELA parameters to a theoretically more benign range: cloud cover throughout the five day period was set to overcast, the roughness length $z_0 = 0.01$, and we use a wind-speed threshold $v_0 = 2.5$ m/s.

The effect of full cloud-cover in the PAMELA model is to make the mid-day local maximum in C_n^2 still less than the overall maximum C_n^2. However it is apparent from fig. 4 that the predicted C_n^2 over the full 48-hour period exceeds the measured values by one to two orders of magnitude. Clearly the dynamic range of PAMELA simulation is excessive for data that is generated in over-water environments, especially considering that a full cloud-cover was invoked.

The PAMELA model predicts that the zero-flux conditions near sunrise and sunset will occur, but this is not seen in the data. This points out a weakness in the current PAMELA model: characteristics such as heat flux at the air-sea interface cannot be represented. The dynamical features in the graph of the PAMELA model in fig. 4 are almost entirely missing in the graph of the recorded infrared data, and in fact a cross-correlation calculation between the model $\log(C_n^2)$ and the measured transmission $\log(C_n^2)$ confirms that the two time series are essentially uncorrelated.
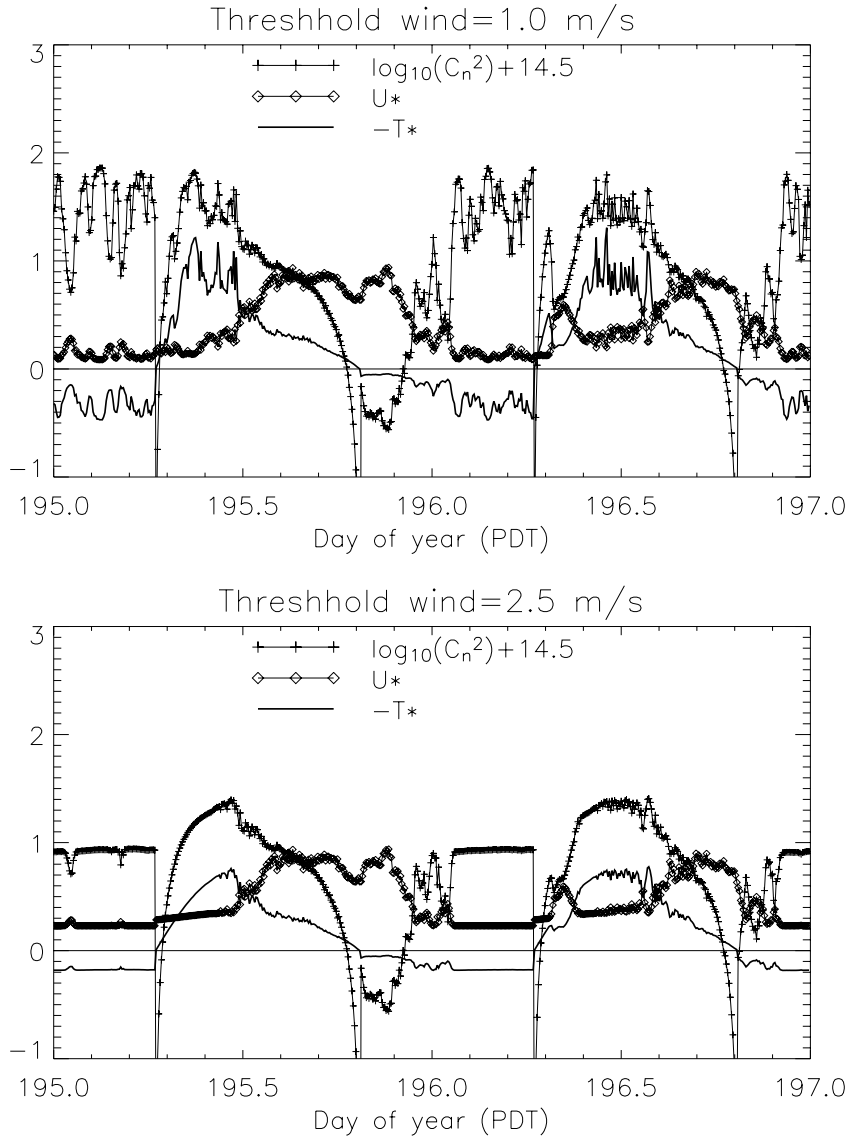
Figure 3. A comparison of T_*, u_*, and C_n^2. For the upper panel, the minimum wind speed threshold is set to 1.0 m/s. In the lower panel, the minimum wind speed threshold is set to 2.5 m/s.

8. THE NAVY SURFACE LAYER OPTICAL TURBULENCE MODEL–NSLOT

The refractive index structure parameter C_n^2 is defined implicitly by the refractive index structure function:

$$\overline{[n(\vec{x}) - n(\vec{x} + \vec{r})]^2} = C_n^2 r^{2/3} \tag{14}$$

where the turbulence is assumed to be isotropic and hence dependent only on $r = |\vec{r}|$.

Optical turbulence is generated by fluctuations in the refractive index n. The derivation of Andreas[3] defines refractive index fluctuations in terms of fluctuations in temperature T and humidity q.

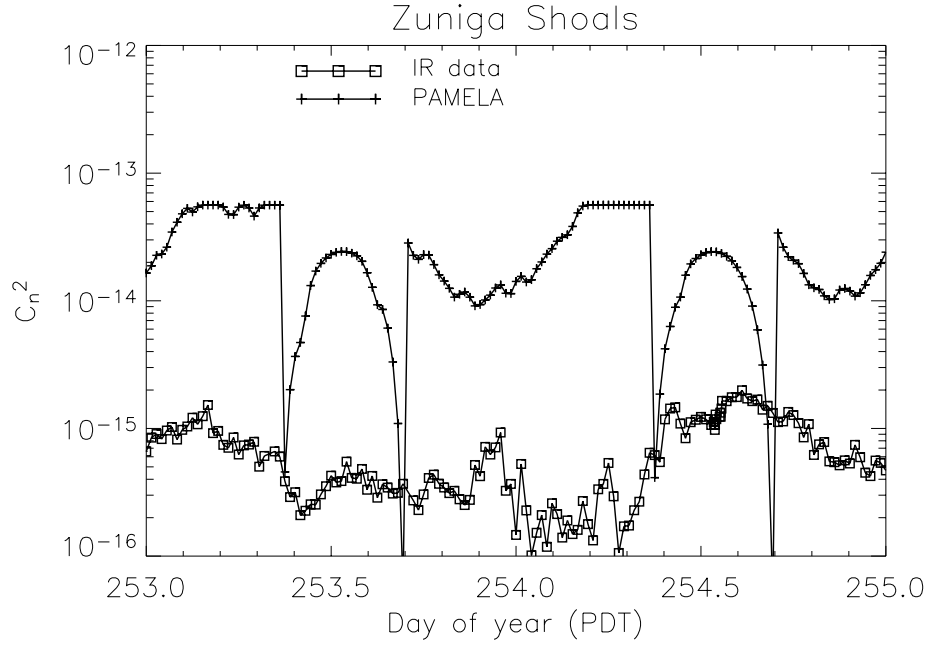$$n' = A(\lambda, P, T, q)T' + B(\lambda, P, T, q)q' \tag{15}$$

Figure 4. A comparison of C_n^2 over the coastal Pacific Ocean for days 253 through 255. Overcast skies (complete cloud cover), a roughness length $z_r = 0.01$ and a threshold wind-speed $v_0 = 2.5$ m/s were used for the PAMELA model.

where a prime indicates an instantaneous turbulent fluctuation of a quantity about its mean value, and

$$A = \frac{\partial n}{\partial T} = -10^{-6} \frac{P}{T^2} \left\{ m_1(\lambda) + [m_2(\lambda) - m_1(\lambda)] \frac{q}{\varepsilon\gamma} \right\} \tag{16}$$

$$B = \frac{\partial n}{\partial q} = 10^{-6} [m_2(\lambda) - m_1(\lambda)] \frac{P}{T\varepsilon\gamma^2} \tag{17}$$

where $\gamma = 1 + 0.6078q$, ε is the ratio of ideal gas constants for dry air over water, and

$$m_1(\lambda) = 23.7134 + \frac{6839.397}{130 - \lambda^{-2}} + \frac{45.473}{38.9 - \lambda^{-2}} \tag{18}$$

$$m_2(\lambda) = 64.8731 + 0.58058\lambda^{-2} - 0.007115\lambda^{-4} + 0.0008851\lambda^{-6} \tag{19}$$

with λ given in μm.

With the structure parameter for temperature C_t^2, the humidity structure parameter C_q^2, and the temperature-humidity structure parameter C_{tq}, we follow Andreas[3] and define :

$$C_n^2 = A^2 C_t^2 + 2ABC_{tq} + B^2 C_q^2$$

A method to estimate C_n^2 from routine meteorological observations is available in the Navy Surface Layer Optical Turbulence (NSLOT).[4] Let the Δ-operator denote a mean air-sea difference for a particular meteorological measurement. Thus an 'air' measurement can be made within the surface layer, a small distance above the sea surface, and a second 'sea' measurement taken at the surface to provide the two measurements indicated by the Δ-operator.

$$C_n^2 = \frac{f(\xi)k^2(\overbrace{A^2\Delta T^2} + \overbrace{2ABr_{Tq}\Delta T\Delta q} + B^2\Delta q^2)}{z^{2/3}[\ln(z/z_{0T}) - \Psi_T(\xi)]} \tag{20}$$
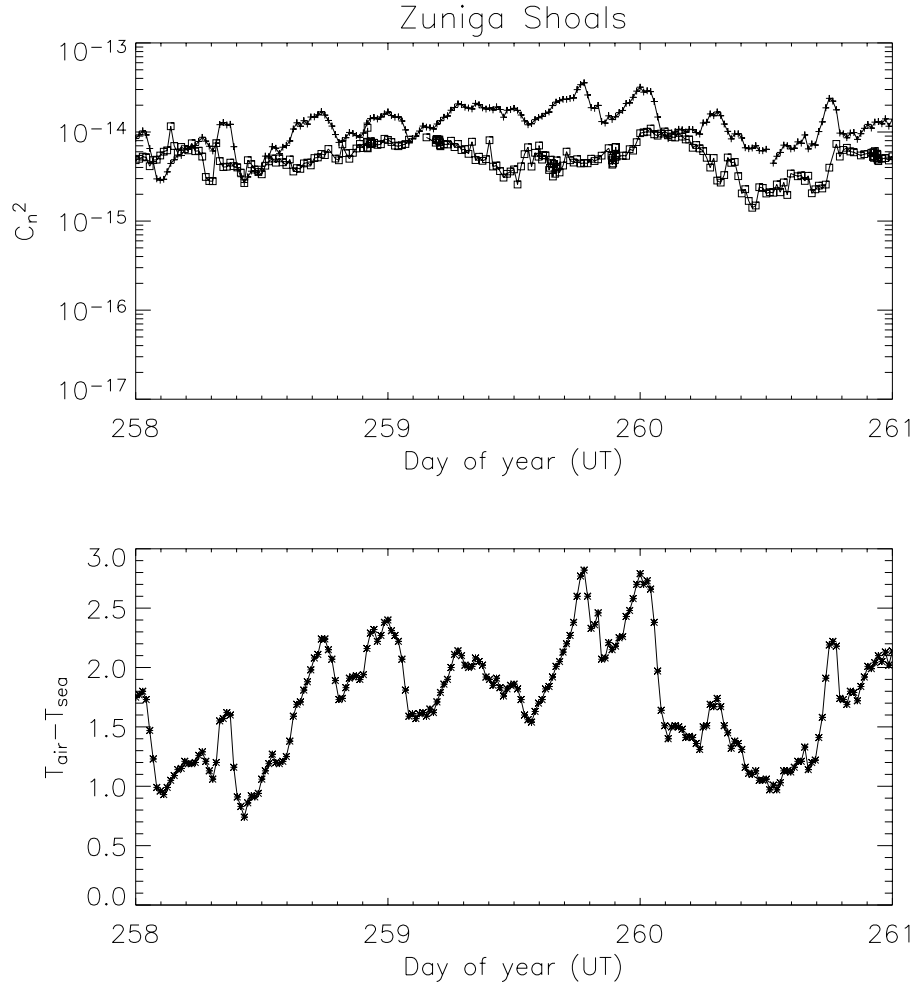
Figure 5. The upper panel shows a comparison of C_n^2 calculation with mid-wave infrared propagation data over Zuniga Shoals (a 7 km over-water path) shown with squares, and the NSLOT model prediction shown with '+' signs. The lower panel follows $\Delta T = T_{\mathrm{air}} - T_{\mathrm{surface}}$ for the same time period.

where z_{0T} is the temperature roughness length, r_{Tq} is the temperature-specific humidity correlation coefficient, $\Psi_T(\xi)$ is a dimensionless profile function, and

$$f(\xi) \equiv f_T(\xi) = f_{Tq}(\xi) = f_q(\xi) = \begin{cases} 5.9(1 - 8\xi)^{-2/3} & \xi \leq 0 \\ 5.9(1 + 2.4\xi^{2/3}) & \xi \geq 0 \end{cases} \tag{21}$$

where

$$\xi = \frac{zg(\Delta T + 0.61 T \Delta q)[\ln(z/z_{0U}) - \Psi_U(\xi)]^2}{\theta_v \Delta U^2 [\ln(z/z_{0T}) - \Psi_T(\xi)]} \tag{22}$$

The behavior of the NSLOT model for data generated over water is shown in fig. 5. In the figure, the values of field observations of C_n^2 are compared to predictions of the NSLOT model parameterized from meteorological data taken from a flux meteorological buoy anchored at the mid-point of the propagation path. The lower panel in the figure shows the values of $\Delta T = T_{\mathrm{air}} - T_{\mathrm{surface}}$ over the analyzed period, and for this period, $\Delta T = T_{\mathrm{air}} - T_{\mathrm{surface}} > 0$, and the NSLOT model over-predicts C_n^2 values. It can be seen that predictions by NSLOT (shown as small + signs) are in general larger C_n^2 than the measured values (seen as plotted squares).
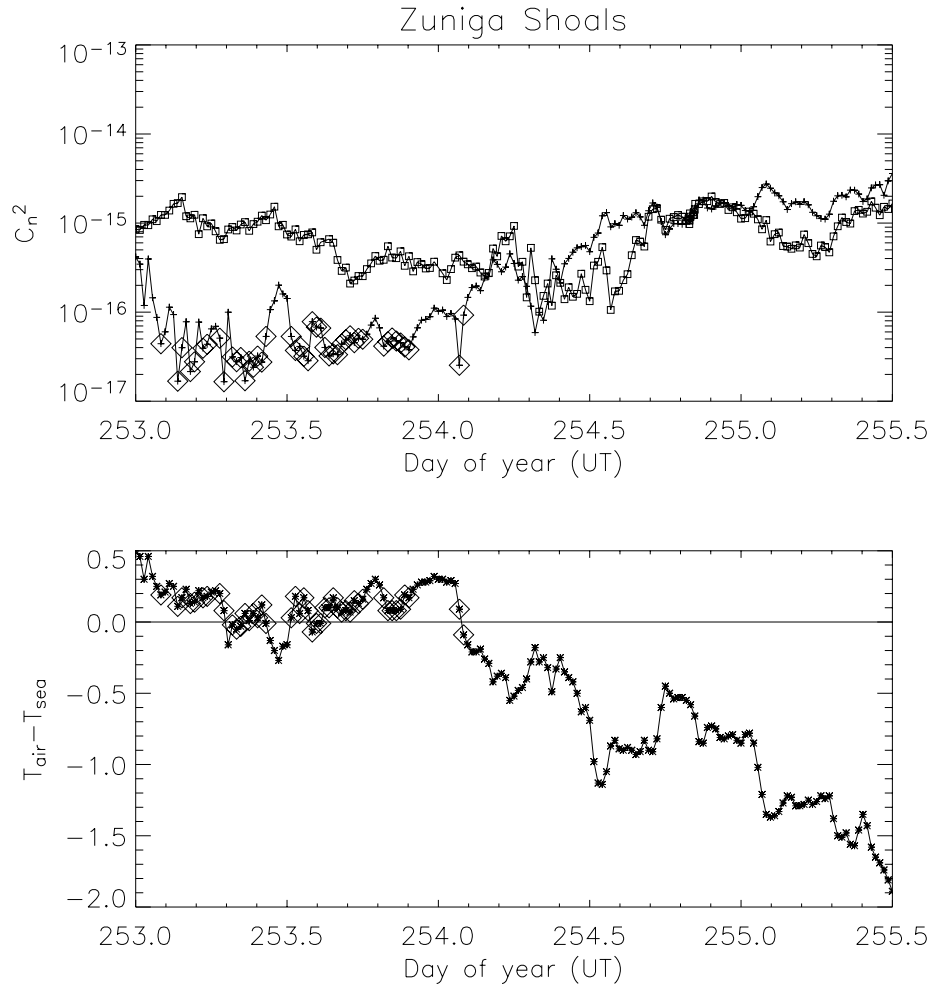
Figure 6. The upper panel shows a comparison of C_n^2 calculation with mid-wave infrared propagation data over Zuniga Shoals shown with squares, and the NSLOT model prediction is shown with '+' signs. The lower panel follows $\Delta T = T_{\text{air}} - T_{\text{surface}}$ for the same time period. Data points satisfying $-0.1 \leq \Delta T = T_{\text{air}} - T_{\text{surface}} \leq 0.2$ are over-plotted with a diamond in both panels.

In figure 6 is shown a comparison of NSLOT predictions with scintillation measurements at a different period of 2.5 days earlier in the same test. For the first day (253.0–254.0), $\Delta T = T_{\text{air}} - T_{\text{surface}} \approx 0$, and this causes NSLOT to predict excessively small values of C_n^2. This behavior can be seen in eqn.(20) by noting that the two terms highlighted with over-brackets go to zero as $\Delta T \to 0$.

To illuminate in fig. 6 how the near-zero values generate poor C_n^2 estimates in NSLOT, the points satisfying $-0.1 \leq \Delta T = T_{\text{air}} - T_{\text{surface}} \leq 0.2$ are over-plotted with a diamond both in the lower panel and in the upper panel. Those points near zero correspond to $10^{-17}\text{m}^{-2/3} \leq C_n^2 \leq 10^{-16}\text{m}^{-2/3}$, and these points deviate from the measured values in some cases by more than a factor of ten. The general trend is for the NSLOT model to under-predict the measured C_n^2 values for ΔT near zero.

In the remaining 1.5 days, (254.0–255.5) the NSLOT model does quite well at predicting the observed C_n^2 values. Thus NSLOT is successful at prediction when the conditions are in a condition common to the open-ocean: $\Delta T = T_{\text{air}} - T_{\text{surface}} < 0$. This provides a striking contrast with the PAMELA model which was compared to the same data (253.0–255.0) as shown in fig. 4.

9. DISCUSSION OF THE NSLOT MODEL

As noted above the NSLOT model performs well for a common open-ocean condition: $\Delta T = T_{air} - T_{surface} \leq \delta_u$ where for example $\delta_u = -0.4°C$. The model also appears to over-predict for $\Delta T = T_{air} - T_{surface} > \delta_s$, where for example $\delta_s = 0.6°C$. (The selections for δ_u and δ_s are simple rough estimate guided by evidence from Frederickson[4]). For the in-between region $\delta_s < \Delta T = T_{air} - T_{surface} < \delta_u$ NSLOT tends to under-predict, sometimes by several orders of magnitude.

10. CONCLUSIONS

We have tested two surface layer optical turbulence models, PAMELA and NSLOT, both of which have been developed from surface layer similarity theory. The first model, PAMELA, is a relatively simple model to implement. However, there are two problems that appeared in the PAMELA test. First, the model is highly sensitive to low wind-speeds. The second problem is the lack of a surface characterization in PAMELA, which prevents a successful prediction for maritime conditions. We are unable to adjust parameters in the model to yield an accurate scintillation prediction for marine propagation conditions.

NSLOT has been developed specifically for the marine environment, and because of this certain parameter values such as surface roughness have been 'hard-wired' into the model. For this reason we did not test the model against over-land data in this report. In tests against over-water data we found that NSLOT can badly under-predict for $\Delta T = T_{air} - T_{surface} \approx 0$. As we indicated in the section above, the source of the difficulty can be seen in over-bracketed terms of eqn. (20). As $\Delta T \rightarrow 0$, the two terms containing ΔT become negligible compared to $B^2 \Delta q^2$. A more detailed study of this weakness in NSLOT is presented in the paper by Frederickson et al.[4]

The NSLOT model is in general a more accurate model for marine propagation conditions. In comparing NSLOT to PAMELA, it is important to note that NSLOT manages the small wind-speed regime more successfully than PAMELA. It is apparent that the NSLOT approach to capturing the surface heat flux by means of T_{air} and $T_{surface}$ measurements and thence a direct determination of $T_{air} - T_{surface}$ is preferable to PAMELA's use of a computed heat flux via solar insolation.

Both models are ultimately constrained by the limitations of surface layer similarity theory. In particular, the theory requires wind speeds that are not too small, and a surface layer of sufficient thickness to encompass the air temperature, humidity, and wind-speed measurements. Conditions that include a temperature inversion or $T_{air} - T_{surface} > 0$ will be problematic for both models.

11. ACKNOWLEDGEMENTS

REFERENCES

1. S.P. Arya, *Introduction to Micrometeorology*, Academic Press, Inc., San Diego, 1988.
2. "Optical Turbulence Model for Laser Propagation and Imaging Applications", draft.
3. E. L. Andreas, "Estimating C_n^2 over snow and sea ice from meteorological data", *J. Opt. Soc. Am. A*, **5**, 481–495, (1988).
4. P. A. Frederickson, K. L. Davidson, C. R. Zeisse, C. S. Bendall, "Estimating the Refractive Index Structure Parameter (C_n^2) over the Ocean Using Bulk Methods", *J. Appl. Meteorology*, **39**, 1770-1783, (200).